A New Volcanic Seismic Signal Descriptor and Its Application to a Data Set From the Cotopaxi Volcano

Noel Pérez, *Member, IEEE*, Pablo Venegas, Diego Benítez, *Senior Member, IEEE*, Román Lara-Cueva, *Senior Member, IEEE*, and Mario Ruiz

***Abstract*— This article proposes a new volcano seismic signal descriptor for improving the area under the receiver operating characteristic curve (AUC) in the classification of long-period (LP) and volcano-tectonic (VT) seismic events. It aims to describe a volcanic seismic event from a different and novel point of view that involves image processing techniques instead of classical seismic signal processing strategies, such as frequency or scale analysis. The proposed descriptor allows exploring the seismic signal space for obtaining the determination of the event patterns and, subsequently, the extraction of intensity-, shape-, and texture-based features into a numeric vectorial output for supplying a set of selected machine learning classifiers with different taxonomies. The descriptor was validated on a seismic signal database collected at the Cotopaxi volcano, containing a total of 637 events, including LP, VT, and other types of seismic events (e.g., rockfall or icequakes). An accuracy value of 96% was obtained in the determination of the event patterns using the signal database, while the values of 0.95 and 0.96 were obtained for the AUC when using a feedforward backpropagation artificial neural network classifier on two experimental data sets, containing feature vectors representing signal with and without event overlapping, respectively. The obtained results demonstrate that the proposed descriptor is capable of providing adequate seismic signal representations in a different feature space and that its output provides competitive results in the classification of volcanic seismic events.**

***Index Terms*— Machine learning classifiers (MLCs), seismic event classification, seismic pattern generation, spectrogram based features.**

Manuscript received August 28, 2019; revised November 20, 2019; accepted February 20, 2020. Date of publication March 12, 2020; date of current version August 28, 2020. This work was supported in part by the Universidad San Francisco de Quito through the Poli-Grants Program under Grant 10100, Grant 12494, and Grant 16916 and in part by the Universidad de las Fuerzas Armadas—ESPE under Grant 2013-PIT-014 and Grant 2016-EXT-038. *(Corresponding author: Diego Benítez.)*

Noel Pérez, Pablo Venegas, and Diego Benítez are with the Colegio de Ciencias e Ingenierías "El Politécnico," Universidad San Francisco de Quito (USFQ), Quito 170157, Ecuador (e-mail: dbenitez@usfq.edu.ec).

Román Lara-Cueva is with the Grupo de Investigación en Sistemas Inteligentes (WiCOM-Energy), Universidad de las Fuerzas Armadas—ESPE, Sangolquí 171103, Ecuador, and also with the Departamento de Eléctrica, Electrónica y Telecomunicaciones, Centro de Investigaciones de Redes Ad-Hoc (CIRAD), Universidad de las Fuerzas Armadas—ESPE, Sangolquí 171103, Ecuador.

Mario Ruiz is with the Instituto Geofísico, Escuela Politécnica Nacional, Quito 170109, Ecuador.

Color versions of one or more of the figures in this article are available online at http://ieeexplore.ieee.org.

Digital Object Identifier 10.1109/TGRS.2020.2976896

I. Introduction

COMPREHENSIVE monitoring of volcanoes is crucial to detect behavioral changes and provide early warnings in the case of imminent volcanic activity. Seismicity, volcanic gases, ground movements, rock and water chemistry, and satellite images should be analyzed to fully understand a volcano's behavior [1]. Although broad monitoring networks comprising several instruments are required for providing information about possible volcanic unrest, seismicity provides meaningful information about the internal activity of volcanoes. The interpretation of the seismic signals can be associated with volcanic processes, such as pressure changes in the system (volcano-tectonic (VT) events), resonating fluid-filled conduits or cracks (long-period (LP) events), magma, ash and gas extrusion (explosions), and long-duration release of energy related to magma degassing (tremors) [2]. In the literature, several machine learning classifiers (MLCs) have been used for the pattern recognition problem associated with the identification of different types of seismic signatures related to volcanic activity. Machine learning approaches usually use some kind of alternative representation of data with respect to the original space, which is obtained by extracting key characteristics from the original signal with the aim of reducing the dimensionality of data and increasing distinction among different classes. Traditionally, features related to specific characteristics in the temporal, frequency, and/or scale and cepstral domains have been used for automatic classification of volcanic-seismic signals [2]–[4]. Statistical features, for example, describe the behavior of the data as a distribution [2], [5], [6], while in the frequency and scale domains, amplitude levels in certain frequency bands have been used as features related to the energy or entropy of the signals [6], [7]. Other features related to the event shape, such as the ratio of values associated with the signal, have also been used as descriptors [2], [6]. However, the optimal representation of seismic events for improving the classification performance remains a persistent problem since several alternative representations of the data with respect to the original space can be used and their effectiveness will depend both on the problem at hand and on the algorithm to be used.

The contribution of this article is to propose a new volcanic seismic signal descriptor for improving the area under the

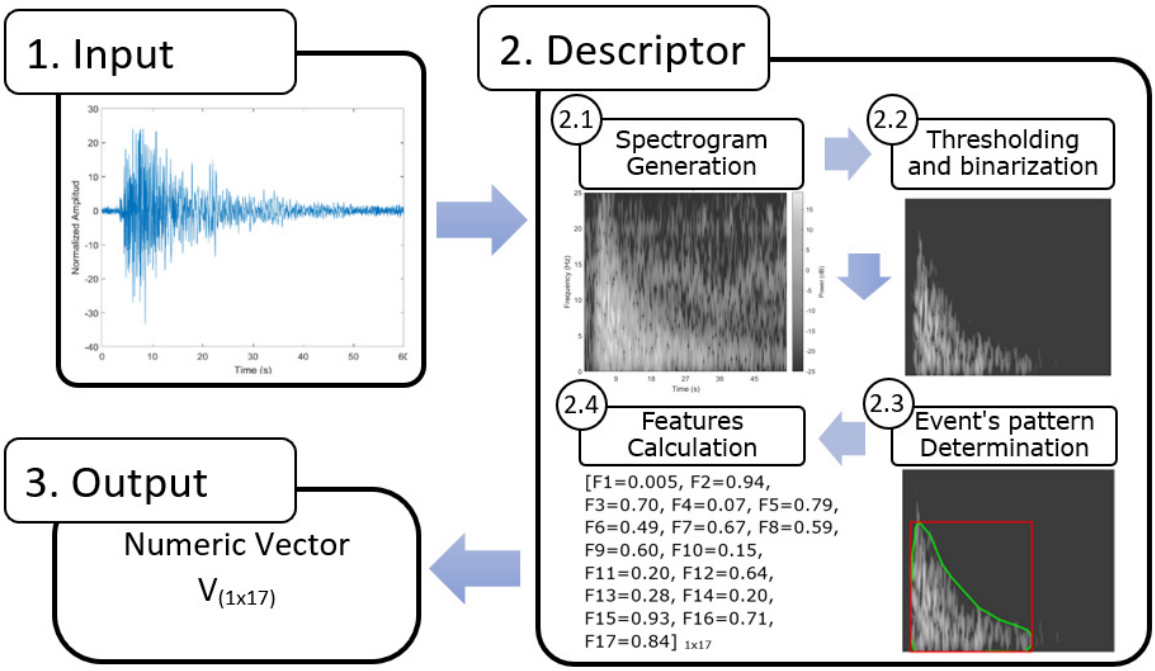

Fig. 1. Workflow of the proposed descriptor.

receiver operating characteristic curve (AUC) in the classification of LP and VT seismic events. The proposed descriptor is aimed to represent the volcanic seismic events from a different and novel point of view that involves image processing techniques instead of classical seismic signal processing strategies, such as frequency or scale analysis. The main idea behind this contribution is twofold: first, the seismic event pattern is segmented into a gray-level spectrogram image, and second, the segmented event image is used to compute a set of 17 features from the intensity statistics, shape, and texture, which are considered as the descriptor output.

This article is organized as follows. Section II presents a detailed description of the proposed descriptor, a brief description of the selected MLCs, and the experimental setup designed for the descriptor evaluation. Section III outlines the accuracy results in the seismic event pattern determination and the descriptor output validation, which was based on the AUC scores obtained by the selected MLCs using the Wilcoxon statistical test [8], [9] for evaluating the importance of the differences between the classification models. Furthermore, an exploratory comparison between the selected MLCs and previously developed approaches available in the literature is presented. Finally, conclusions and future work are summarized in Section IV.

II. Materials and Methods

A. Seismic Signal Database

The database used in this article contains 637 seismic events, in which 560 and 77 samples belong to LP and VT classes, respectively. All the data were acquired during 2012, January 2013, January 2014, January 2018, and between the months of January 2019 and March 2019 from the Cotopaxi volcano (00.677 °S, 78.436 °W) in Ecuador. This database was provided by the Geophysical Institute of National Polytechnic School (Instituto Geofísico de la Escuela Politécnica Nacional) (IGEPN), which is responsible for monitoring and analyzing seismic and volcanic activity in Ecuador. The broadband seismic acquisition system used a three-axial seismometer (CMG-40T Guralp) with a sensitivity of 1600 V/ms^{-1} and a 24-bit analog-to-digital converter (Geotech Smart 24-D digitizer), sampling at 50 Hz. Each seismogram from this database contains one independent seismic event that was manually identified and labeled by analysts at the IGEPN considering its waveform, spectrogram, and location.

B. Proposed Volcanic Seismic Signal Descriptor

The proposed descriptor aims to represent the input signal into a numeric output vector containing information from the intensity statistics, shape, and texture computed from a delimited region of interest within the spectrogram image. The workflow of the proposed descriptor is shown in Fig. 1, and the description of individual steps are presented as follows.

1) Spectrogram Generation: The gray-level spectrogram images were generated using the short-time Fourier transform (STFT) [10] over the original signal. This process used a Kaiser window [11], [12] with 1.5-s sampling window size and 75% of overlapping to avoid losing information in the boundary of the window (see Fig. 1 step 2.1) and, thus, to maximize the energy in the main part of the signal.

2) Thresholding and Binarization: This step filters the gray-level spectrogram images with an experimentally determined threshold value of 0 dB (see Fig. 1 step 2.2) to remove the frequency components with low magnitude while retaining

those related to the seismic event. The data acquisition system (seismometers) is highly sensitive; therefore, the presence of noise at different frequencies is common, thus, using a power threshold helps to clean the signal. Subsequently, each gray-level scale image was converted to a binary image using Otsu's method [13], which computes the optimum conversion threshold by minimizing the intraclass variance between two assumed pixel classes (see Fig. 1 step 2.2).

3) Determination of the Event Pattern: This step involves determining the contour and bounding box of the area of interest that corresponds to the seismic event. The contour computation was based on the Moore-neighbor tracing algorithm modified by Jacob's stopping criteria [14] (see Fig. 1 step 2.3, green line). On the other hand, the bounding box determination was carried out using the eight-connected components (object or blobs) algorithm (see Fig. 1 step 2.3, red line). It aims to find the contour of objects in an image by placing a seed (initial pixel) and exhaustively scanning the eight-connected pixels around it in a clockwise direction; this process verifies whether or not there are changes in the current pixel intensity with respect to the seed.

4) Feature Calculation: A set of 17 features corresponding to intensity statistics, shape, and texture descriptors were computed from the segmented event patterns. These features were used to form a numeric vector that constitutes the proposed descriptor output. The selected features were considered on the base of previously developed approaches, which found them able to provide relevant information in image classification problems [15]–[17] (see Fig. 1 step 2.4—inside of the green-line contour).

An overview of each computed feature, separated by groups, is presented in the following.

1) *Intensity Statistics-Based Features:* Selected features are related to the pixel intensity statistics [15] of the segmented seismic event patterns, as follows.
   a) *Excess Kurtosis (f_1):*
   $$f_1 = \frac{\frac{1}{n}\sum_{i=1}^{n}(x_i - \bar{x})^4}{\left[\sqrt{\frac{1}{n}\sum_{i=1}^{n}(x_i - \bar{x})^2}\right]^2} - 3.$$
   b) *Maximum (f_2):* The maximum intensity value in the region surrounded by the contour.
   c) *Mean (f_3):*
   $$f_3 = \frac{1}{n}\sum_{i=1}^{n} x_i.$$
   d) *Skewness (f_4):*
   $$f_4 = \frac{\frac{1}{n}\sum_{i=1}^{n}(x_i - \bar{x})^3}{\left[\sqrt{\frac{1}{n}\sum_{i=1}^{n}(x_i - \bar{x})^2}\right]^3}.$$
   e) *Standard Deviation (f_5):*
   $$f_5 = \sqrt{\frac{1}{n-1}\sum_{i=1}^{n}(x_i - \bar{x})^2}$$
   where n is the number of pixels inside the region delimited by the contour, x_i is the gray-level intensity of the ith pixel inside the contour, and $\bar{x}$ is the mean sample intensity.
2) *Shape-Based Features:* Selected features are related to the contour and bounding box where the seismic event is embedded, as follows.
   a) *Area (f_6):* $f_6 = |O|$.
   b) *Perimeter (f_7):* $f_7 = length(E)$.
   c) *Circularity (f_8):*
   $$f_8 = 4\pi \frac{\text{area}}{\text{perimeter}^2}.$$
   d) *Elongation (f_9):* $f_9 = (m/M)$.
   e) *Shape (f_{10}):*
   $$f_{10} = \frac{\text{perimeter} * \text{elongation}}{8 * \text{area}}.$$
   f) *X Center of Mass (f_{11}):* Normalized X coordinates of the center of mass of O.
   g) *Y Center of Mass (f_{12}):* Normalized Y coordinates of the center of mass of O.

   Here, O is the set of pixels that belong to the segmented seismic event pattern, $E \subset O$ is the edge pixels, m is the minor axis, and M is the major axis of the ellipse that has the same normalized second central moments as the region surrounded by the contour.
3) *Texture-Based Features:* Selected features are based on Halarick's descriptors extracted from the gray-level co-occurrence matrices [18].
   a) *Angular Second Moment* (f_{13}):
   $$f_{13} = \sum_{i=1}^{L}\sum_{j=1}^{L} p(i,j)^2.$$
   b) *Contrast* (f_{14}):
   $$f_{14} = \sum_{i}\sum_{j} p(i,j)(i-j)^2.$$
   c) *Correlation* (f_{15}):
   $$f_{15} = \frac{\sum_i \sum_j [ijp(i,j)] - \mu_x \mu_y}{\sigma_x \sigma_y}.$$
   d) *Entropy* (f_{16}):
   $$f_{16} = \sum_{i=1}^{L}\sum_{j=1}^{L} p(i,j) log(p(i,j)).$$
   e) *Inverse Difference Moment* (f_{17}):
   $$f_{17} = \sum_{i}\sum_{j} \frac{1}{1+(i-j)^2} p(i,j).$$

where L is the number of gray levels, and $p(i,j)$ is the probability that the pixels with the gray level i appear next to the pixels with the gray level j, while μ_x and μ_y are the means, and σ_x and σ_y are the standard deviations of the marginal distribution associated with $p(i,j)$.

C. Machine Learning Classifiers

Several MLCs have been reported in the literature for seismic event classification. Variations of the support vector machine (SVM) method seem to be the most widely used type of classifier, e.g., SVM with linear kernel [19], [20] and multiclass SVM [20]–[22]. Other less popular methods that have been performed satisfactorily are artificial neural networks (ANNs) [22], [23], decision trees [19], [24], hidden Markov models [25], evolutionary algorithms [26], [27], and, more recently, Gaussian mixture model [28]. Thus, five MLCs with different taxonomies (depending on their functionality) were considered in this article to perform a fair evaluation of the proposed descriptor output. The selected MLCs are briefly described as follows.

1) Naive Bayes (NB) Classifier: The NB classifier is based on probabilistic models with strong (naive) independence assumptions [29]. It assumes that c is a class variable depending on n input features: $x_1, x_2, \ldots, x_n$. The prediction of the class variable c is based on the conditional model of Bayes' theorem for a constant denominator when features are given (it does not depend on c). Thus

$$p(c|x_1, x_2, \ldots, x_n) = \frac{1}{z} p(c) \prod_{i=1}^{n} p(x_i|c)$$

where z is a normalization constant. After being trained in the NB classifier (estimating the class priors and the probability distribution of features), any test sample will follow the decision rule that provides the most probable value of c (the maximum *a posteriori* of the model).

2) SVM Classifier: SVMs are based on the definition of an optimal hyperplane, which linearly separates the training data. In comparison with other classification methods, an SVM aims to minimize the empirical risk and maximize the distances (geometric margin) of the data points from the corresponding linear decision boundary [30].

3) k-Nearest Neighbors (kNNs) Classifier: The kNNs classifier is a nonparametric technique that employs a little effort into building the classifier (lazy learning). It assigns a test sample to the class of the majority of its k-neighbors, that is, assuming that the number of voting neighbors is $k = k_1 + k_2 + \cdots + k_n$ (where n is the number of samples from class i in the k-sample neighborhood of the test sample, usually computed using the Euclidean distance), the test sample is assigned to class m if $k_m = \max(k_i), i = 1, 2, \ldots, n$ [31].

4) Feedforward Backpropagation (FFBP) Neural Network Classifier: The FFBP neural network is a particular model of ANN, which provides a nonlinear mapping between its input and output according to the backpropagation error learning algorithm. This model has demonstrated to be capable of approximating an arbitrarily complex mapping within finite support using only a sufficient number of neurons in few hidden layers (all layers using a sigmoid function as kernel type) [32].

5) Random Forest (RF) Classifier: The RF is an ensemble algorithm based on the combination of several tree predictors (empirical selection). The model input (feature vector) is randomly divided into several feature vectors (with the same distribution) for feeding each tree. The obtained classification results by the employed trees are used to calculate the statistical mode of results, which is the output of the RF classifier [33].

D. Experimental Setup

This section outlines the experimental evaluation of the proposed descriptor using a seismic signal database containing LP and VT seismic events. The validation was based on two main stages: first, the proof of concept of the events pattern determination, which aims to guarantee a satisfactory segmentation of the seismic event in the gray-level spectrogram images, and second, the performance of the descriptor output in the classification of seismic events using five different MLCs.

1) Proof of Concept of the Events Pattern Determination: The proof was mainly designed to verify the satisfactory segmentation of the seismic event pattern, as well as its adequate bounding box determination. A correct segmentation and bounding box calculation is achieved if the event pattern area is within both curves, respectively. A good segmentation and bounding box determination are necessary to avoid a wrongly feature calculation. Therefore, closed curves should be obtained for all events under analysis.

2) Quality of the Descriptor Output: This test intended to validate the proposed descriptor output and to gather relevant information about the quality of computed features. In such a sense, five different MLCs, NB, SVM, kNN, FFBP ANN, and RF classifiers, were used in combination with the descriptor output. The performance results of the selected MLCs will provide evidence on how good the descriptor output is in terms of seismic events classification. The training and test partitions, MLCs configuration, and assessment metrics employed in the test are described as follows.

1) *Training and Test Partitions:* The seismic signal database was used as input to the proposed descriptor for creating an experimental data set of feature vectors, where each vector contains the resulting representation of the input seismic signal in terms of intensity statistics, shape, and texture. Since each input signal produced a numeric vector output, the experimental data set will contain a total of 637 feature vectors (560 LP and 77 VT). In particular, we applied ten times the tenfold cross-validation method [34] before the classification step to form disjoint training and test partitions. In this way, individual MLCs will be trained on different training sets and, thus, learning from different input space representations. Testing on these different sets leads to variability in the resultant classification for individual samples.
2) *MLCs Configuration:* For all MLCs, except for the NB (which is parameterless), the tenfold cross-validation method [34] was performed on the training set for optimizing the MLCs parameters. The SVM classifier used the regularization parameter C (cost) optimized in the range from 10^{-4} to 10^{4} (increasing by a factor of 10), and the kernel function was tuned to be linear, radial basis, polynomial, and sigmoid functions. The

kNN classifier involved the estimation of an optimal value of k in determining the size of the neighborhood. The k value was optimized in the range from 1 to 20, and the contribution of neighbors always used the weighted Euclidean distance to the instance being classified. The FFBP neural network used a total of n hidden layers determined by the formula $n = (\text{attributes} + \text{number of classes})/2$. One output layer associated with the binary classification (LP or VT). The transfer function for all layers employed the sigmoid (hyperbolic tangent) function, and the number of iterations (epochs) was optimized in the interval from 100 to 10 000 epochs with an interval increment of 500 units. The RF classifier included the selection of an optimal number of tree-based predictors, which was optimized between 100 and 1000 (with an increment of ten units). Each tree used the $\log_2(X) + 1$ for randomly attributes selection, being X the total number of attributes available in the current data set.

3) *Assessment Metrics:* The determination of the event pattern and the correct segmentation and delimitation of the bounding box were evaluated using the accuracy (ACC) metric. This metric was also used to support the comparison against previously developed approaches, which provided their results based on the ACC metric. On the other hand, for evaluating the MLCs performance, the AUC metric was used. Moreover, we used the Wilcoxon statistical test [8], [9] one time per comparison to assess the importance of the differences between classification models.

The implementation and application of the proposed descriptor were made in MATLAB (Release R2019a) [35], while the employed MLCs are available in the WEKA data mining software (version 3.6) [36].

III. Results and Discussion

A. Performance of the Proposed Descriptor

In most cases, the determination of the event pattern was successful. We obtained an ACC value of 96%, corroborating the satisfactory performance of the descriptor for the segmentation of LP and VT seismic events. Figs. 2 and 3 show examples of the obtained results for both cases. From both figures, it is possible to observe that the green (segmented pattern) and red (bounding box) contour lines are well-closed curves containing the event pattern (Figs. 2 and 3, fourth column), thus ensuring an appropriate calculation of the features (Figs. 2 and 3, fifth column).

Despite the satisfactory results obtained, there was an overall failure of 4% for both types of events. In these cases, the descriptor performed the segmentation and the delimitation of the bounding box without taking into consideration other objects present in the image. Eventually, this situation leads to an incorrect segmentation and, therefore, to an incorrect calculation of features. This effect is mainly associated with overlapped signals that could occur at the same time or immediately after the event occurrence. For example, during an LP or VT event, a rockfall or an icequake may occur, which produces a mixed signal that was recorded by the seismometers (see Figs. 4 and 5).

Concerning the variation of the morphology of the event patterns, it is interesting to note that the LP events are smaller in amplitude than the VT events. Meanwhile, the box width depends on the duration of the event, which means that it varies from case to case. For example, in Figs. 2 and 3, both events retain a similar width throughout the sampling window, different than the situation shown in Figs. 4 and 5. These morphological differences are also expressed when comparing the descriptor output for LP and VT events.

We discuss these differences for the examples presented in the first row of Figs. 2–5. For successful cases, within the statistics of intensity-based features, except for the excess kurtosis (F_1) and skewness (F_4) features, which seems to provide less variation between both types of events ($\Delta F_1 = 0.004$ and $\Delta F_4 = 0.07$), the value of $F_2 = 0.50$ (maximum), $F_3 = 0.28$ (minimum), and $F_5 = 0.53$ (standard deviation) obtained from LP events versus $F_2 = 0.94$, $F_3 = 0.70$, and $F_5 = 0.79$ reached by the VT events represented a significant variation of $\Delta F_2 = 0.44$, $\Delta F_3 = 0.42$, and $\Delta F_5 = 0.26$ units. The small variations in the F_1 and F_4 features were expected since they represent the fourth (sharpest peaks of the distribution) and third (left or right skewed distribution) moments of the gray tone distribution, and since these features are calculated in gray-level images, they will contribute to a lower degree of variation (see Figs. 2 and 3, fifth column).

For the shape-based features group, on the other hand, the perimeter (F_7) is the feature with less variance between both type of events ($\Delta F_7 = 0.08$). This value is a result of the considered examples. Although it is possible to observe that the VT events are morphologically higher than the LP events, this situation is not the same with the width, which depends on the duration of the event. Therefore, there is not always a relationship between both properties that normally have small values. In addition, the value of $F_6 = 0.26$ (area), $F_8 = 0.35$ (circularity), $F_9 = 0.15$ (elongation), $F_{10} = 0.03$ (shape), $F_{11} = 0.39$ (x center mass), and $F_{12} = 0.96$ (y center mass) obtained for LP events versus $F_6 = 0.49$, $F_8 = 0.59$, $F_9 = 0.60$, $F_{10} = 0.15$, $F_{11} = 0.20$, and $F_{12} = 0.64$ obtained for VT events indicate a significant variation of $\Delta F_6 = 0.23$, $\Delta F_8 = 0.24$, $\Delta F_9 = 0.45$, $\Delta F_{10} = 0.12$, $\Delta F_{11} = 0.19$, and $\Delta F_{12} = 0.32$ units (see Figs. 2 and 3 fifth column).

Within the group of texture-based features, the second angular momentum (F_{13}) and the contrast (F_{14}) appeared as the features with less variance between both type of events ($\Delta F_{13} = 0.02$ and $\Delta F_{14} = 0.07$). These results were expected since the F_{13} measures how homogeneous is the intensity of an image, and for a gray-level image, there are very few dominant gray-tone transitions. Similarly, the F_{14} feature is related to the amount of local intensity variation presented in the image, which is irrelevant on gray-level images. Moreover, the value of $F_{15} = 0.69$ (correlation), $F_{16} = 0.38$ (entropy), and $F_{17} = 0.72$ (inverse difference moment) of LP events versus $F_{15} = 0.93$, $F_{16} = 0.71$, and $F_{17} = 0.84$ achieved from VT events implied a significant variation of $\Delta F_{15} = 0.24$, $\Delta F_{16} = 0.33$, and $\Delta F_{17} = 0.12$ units (see Figs. 2 and 3, fifth column).

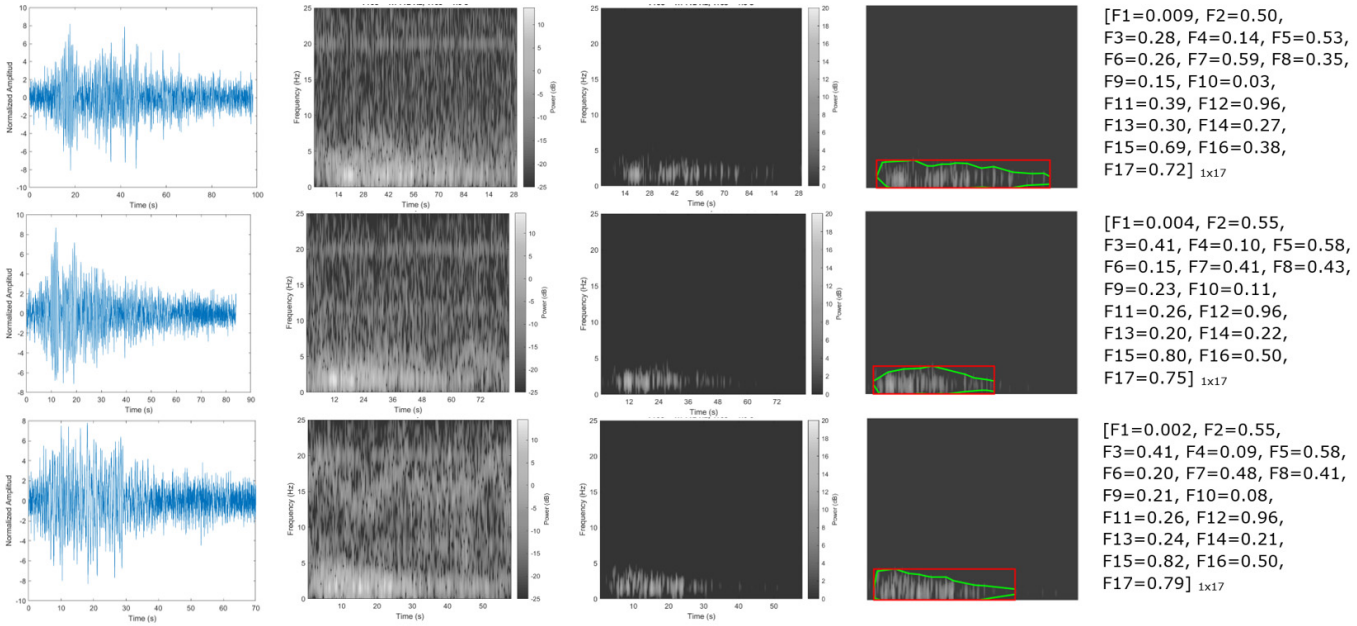

Fig. 2. Examples of successful descriptor performance result using a random selection of three LP seismic events. From left to right: input signal, spectrogram, spectrogram thresholding, image transformation, event's pattern determination, and features calculation.

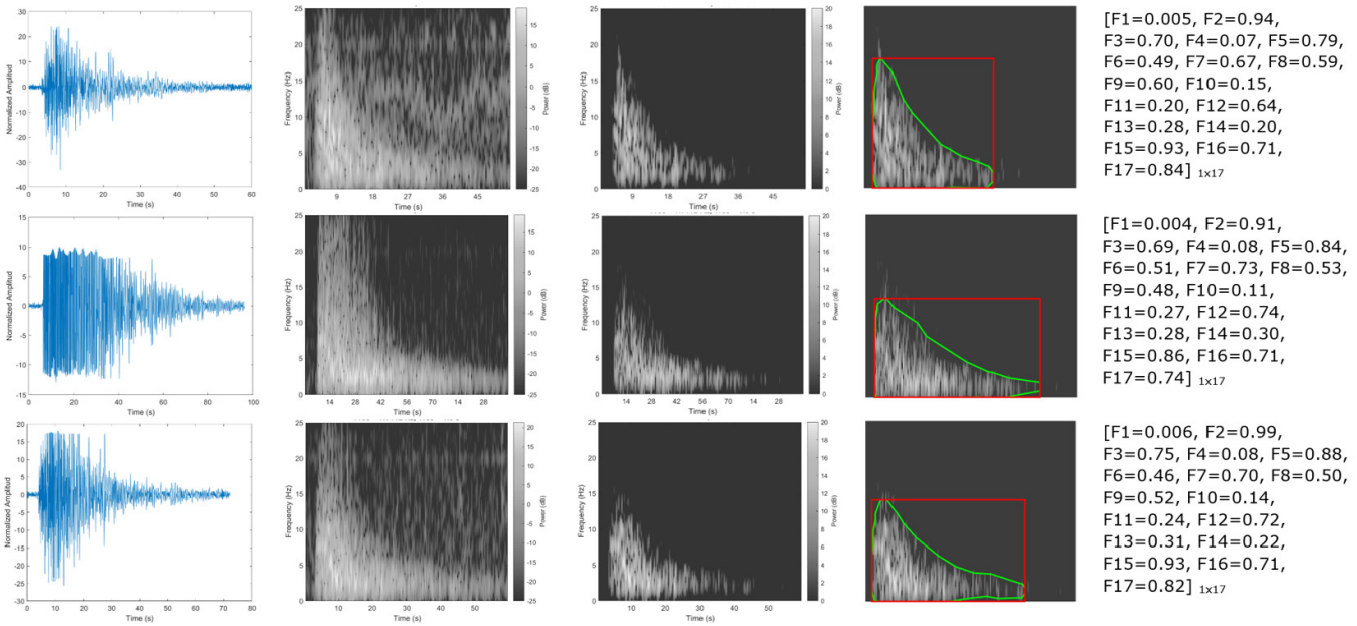

Fig. 3. Examples of successful descriptor performance result using a random selection of three VT seismic events. From left to right: input signal, spectrogram, spectrogram thresholding, image transformation, event's pattern determination, and features calculation.

With regards to the feature variation between successful and unsuccessful cases, it should be noted that the excess kurtosis (F_1), skewness (F_4), second angular moment (F_{13}), and contrast (F_{14}) are features that constantly provide small values of variation between both types of events when calculated from a satisfactory event pattern segmentation, as shown in Figs. 2 and 3, fifth column. On the other hand, when these features were computed from an unsatisfactory event pattern segmentation, only the excess kurtosis and skewness maintained the same performance of small variation values (see Figs. 4 and 5, fifth column). This behavior was expected since these features are prone to be invariant in gray-level images. The second angular momentum (F_{13}) and contrast (F_{14}) features showed a significant increase in the variance between both types of events, whereas other features, such as area (F_6) and correlation (F_{15}), did not. The unsuccessful event pattern segmentation introduces a lack of intensity values (black) between the event pattern and other objects. This effect triggers a local intensity variation that affects the second angular moment (F_{13}) and contrast (F_{14}) features

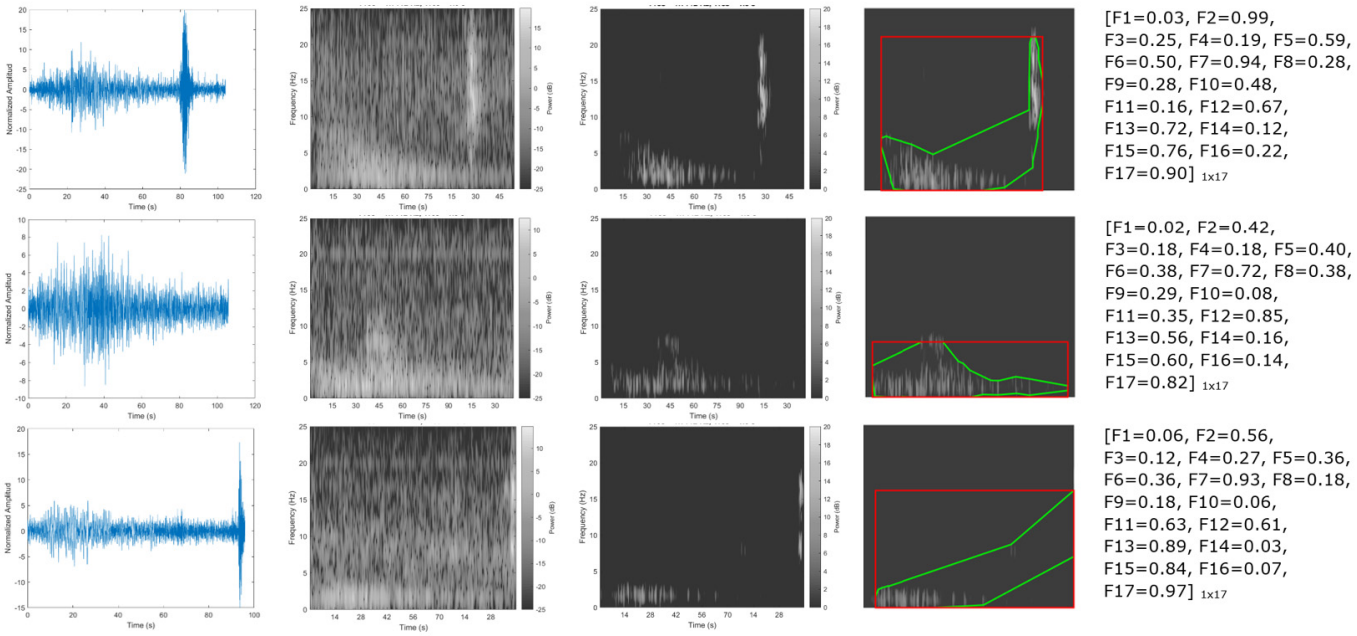

Fig. 4. Examples of unsuccessful descriptor performance result using a random selection of three LP seismic events. From left to right: input signal, spectrogram, spectrogram thresholding, image transformation, event's pattern determination, and features calculation.

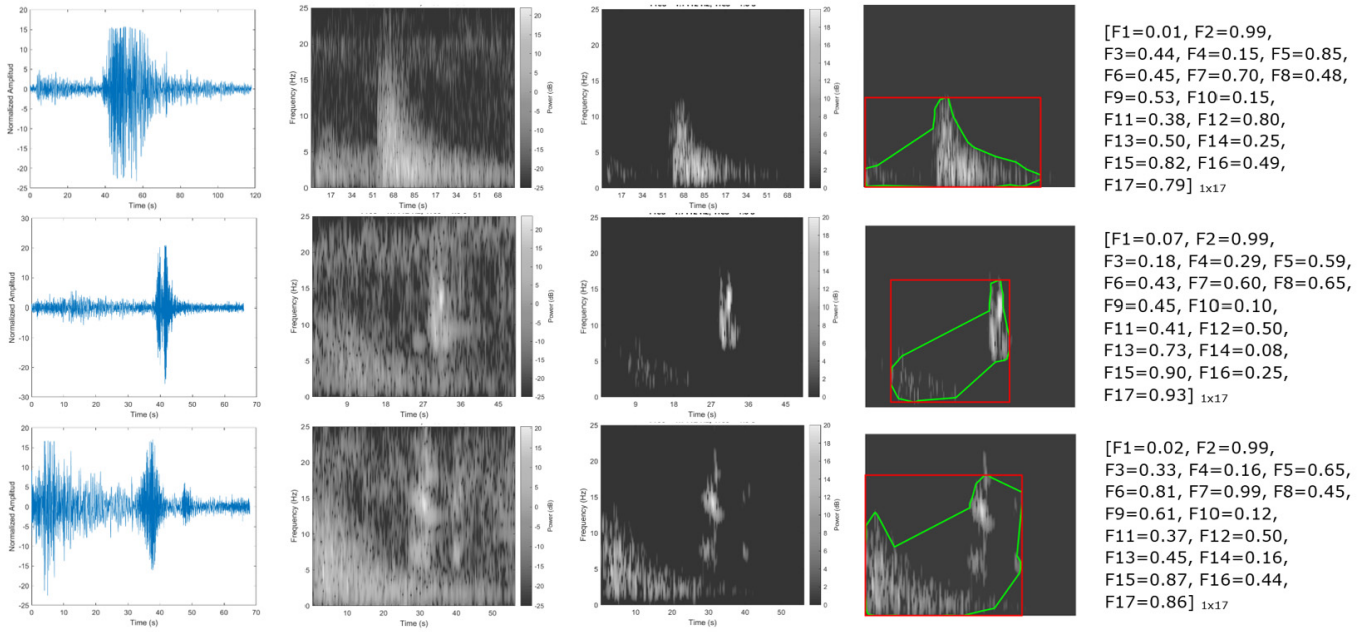

Fig. 5. Examples of unsuccessful descriptor performance result using a random selection of three VT seismic events. From left to right: input signal, spectrogram, spectrogram thresholding, image transformation, event's pattern determination, and features calculation.

and, at the same time, decreases the importance of features such as the area (F_6) and correlation (F_{15}). Therefore, the features resulting from the proposed descriptor depend to a large extent on the correct determination of the event pattern.

B. Quality of the Descriptor Output

We evaluated the descriptor output using five different MLCs on two experimental data sets. The first (D1) was formed with numerical vectors (descriptor outputs) extracted from the input signals that did not contain overlapped seismic events, representing a total of 598 instances. Meanwhile, the second (D2) was created with all the numerical vectors of the D1 data set plus numerical vectors extracted from the input signals that contain overlapped seismic events (i.e., 39 additional instances containing 32 LP and seven VT events), totaling 637 instances. The obtained results by the MLCs are described in the following.

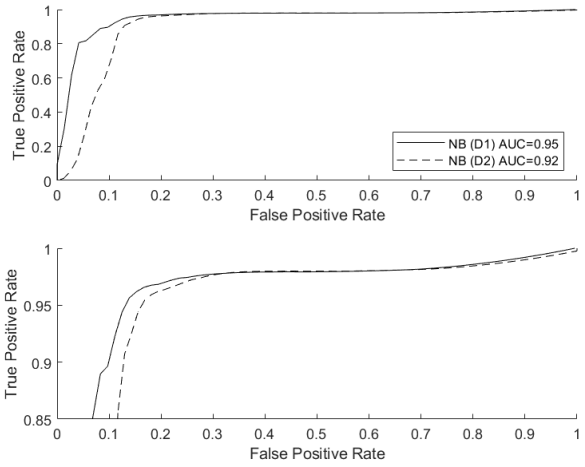

Fig. 6. Classification performance based on the AUC of the NB classifier. (Top graph) ROC curve and (Bottom graph) zoomed-in part of the ROC curve with an AUC $\geqslant 0.85$.

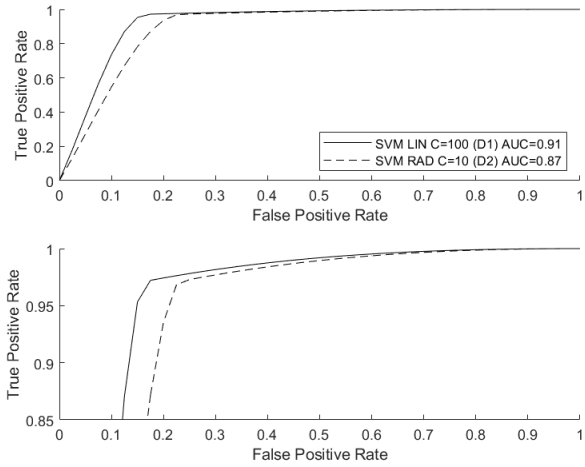

Fig. 7. Classification performance based on the AUC of the SVM classifier. (Top graph) ROC curve and (Bottom graph) zoomed-in part of the ROC curve with an AUC $\geqslant 0.85$.

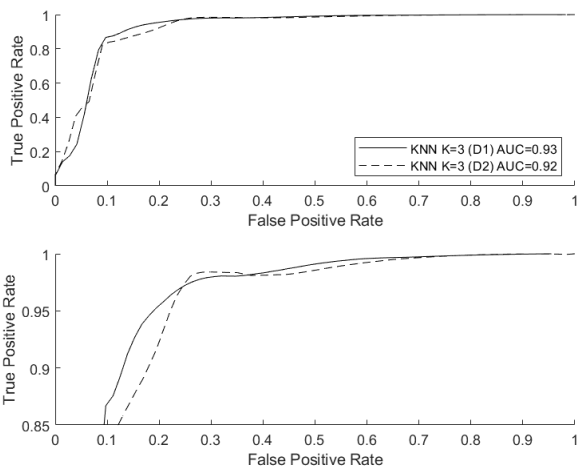

Fig. 8. Classification performance based on the AUC of the kNN classifier. (Top graph) ROC curve and (Bottom graph) zoomed-in part of the ROC curve with an AUC $\geqslant 0.85$.

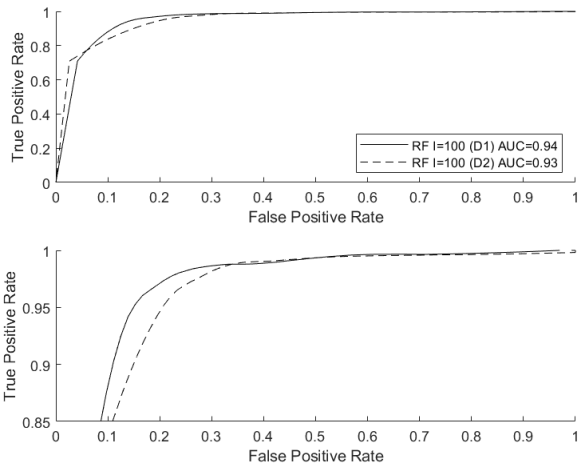

Fig. 9. Classification performance based on the AUC of the RF classifier. (Top graph) ROC curve and (Bottom graph) zoomed-in part of the ROC curve with an AUC $\geqslant 0.85$.

1) NB Classifier Performance: The best result obtained by this classifier in the D1 data set was an AUC value of 0.95, as shown in Fig. 6. However, when used in the D2 data set, the best performance achieved was an AUC value of 0.92 (see Fig. 6). The significant difference in the AUC metric (ΔAUC $= 0.03$ at $p = 0.005$) was mainly due to the superposition of signals presented in the D2 data set. Despite this difference, it is possible to observe satisfactory results provided by this classifier in both data sets.

2) SVM Classifier Performance: The best result of this classifier was obtained by the model formed with a linear kernel and the cost parameter $c = 100$ in the D1 data set, achieving an AUC value of 0.91 (see Fig. 7). In the D2 data set, the best performance was obtained by the model using a radial kernel with the cost parameter $c = 10$. This configuration reached an AUC value of 0.87 (see Fig. 7). The significant variation of AUC (ΔAUC $= 0.04$ at $p = 0.005$) was due to the high sensibility of this classifier to overlapped seismic events presented in the D2 data set.

3) kNN Classifier Performance: This classifier performed similarly on both data sets. The best AUC results were 0.93 and 0.92 using the D1 and D2 data sets, respectively. These results were obtained using the same model with a number of neighbors of $K = 3$ (see Fig. 8). The difference in AUC values (ΔAUC $= 0.01$) was statistically insignificant, demonstrating its potential to overcome the problem with the signal overlapping presented in the D2 data set. Thus, the proposed descriptor output provides satisfactory results when combines with this classifier.

4) RF Classifier Performance: This classifier exhibited a similar performance of classification on both data sets. The model using a total of 100 trees in the forest achieved AUC values of 0.94 and 0.93 on D1 and D2 data sets, respectively (see Fig. 9). The AUC difference of ΔAUC $= 0.01$ in performance between both data sets is statistically negligible at $p = 0.05$. Therefore, the behavior of the descriptor to signal overlapping does not significantly affect the performance of this classifier. Due to the favorable obtained results,

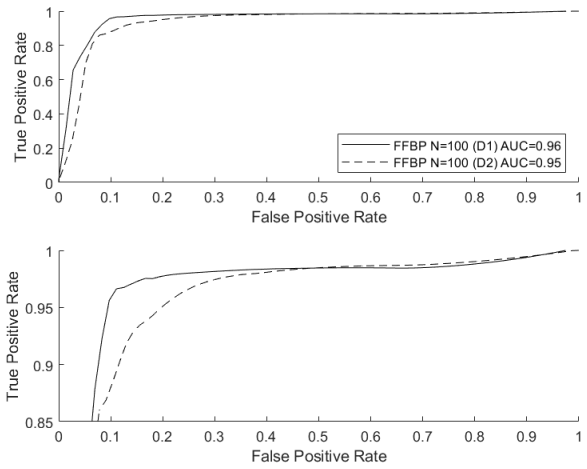

Fig. 10. Classification performance based on the AUC of the FFBP ANN classifier. (Top graph) ROC curve and (Bottom graph) zoomed-in part of the ROC curve with an AUC $\geqslant 0.85$.

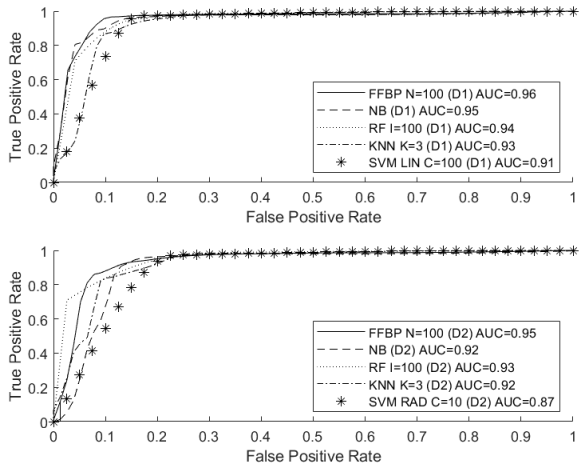

Fig. 11. Best AUC-based classification performance comparison among selected MLCs. ROC curve plot obtained with the (Top row) D1 and (Bottom row) D2 data sets.

it is possible to establish that the proposed descriptor offers satisfactory results when used together with this classifier.

5) FFBP Neural Network Classifier Performance: The best results for this classifier were obtained with a total of $N = 100$ iterations (epoch) on both data sets. It reached an AUC value of 0.96 and 0.95 on the D1 and D2 data sets, respectively (see Fig. 10). The small obtained difference in AUC values ($\Delta\text{AUC} = 0.01$) from both data sets is considered statistically similar at $p = 0.05$. Therefore, it is possible to affirm that the signal overlapping problem does not affect the performance of this classifier, and it can be considered as a good candidate to be combined with the proposed descriptor.

C. Classifiers Performance Comparison

The obtained classification performance by selected MLCs was satisfactory on both experimental data sets. The classifier based on the FFBP ANN achieved the best AUC in the D1 data set with a score of 0.96. This result was statistically similar at $p = 0.05$ compared with the AUC values of 0.95 and 0.94 reached by the NB and RF classifiers, respectively. Other explored classifiers provided interesting AUC scores, such as 0.91 (SVM) and 0.93 (kNN), but they showed inferior statistical performance, as can be seen in Fig. 11, top row. Similarly, for the D2 data set, the FFBP ANN-based classifier also achieved the best AUC score (0.95). However, this result did not provide statistical differences at $p = 0.05$ compared with the NB, RF, and kNN classifiers, which reached AUC values of 0.93, 0.92, and 0.92, respectively. Nonetheless, this score was statistically superior to the AUC score of 0.87 obtained by the SVM classifier (see Fig. 11, bottom row). These results could be supported by the nature of each classifier and the particularity of employed data sets.

It should be noted the variation of the results produced by the overlapped seismic events included in the D2 data set did not significantly alter the performance of the FFBP ANN, NB, RF, and kNN classifiers. Notably, the FFBP ANN-based classifier demonstrated its excellent capability to find a satisfactory decision boundary on both feature spaces (D1 and D2 data sets). The conditional model function used with the NB classifier showed little sensitivity to the data variation, especially with the D2 data set. The RF classifier is composed of several trees (100 units in this article), and a single tree used the information gain criteria for each in-depth level construction. Therefore, as long as each feature contains data variation (entropy), the rules constructed from the tree will be sufficient to provide satisfactory classification results. Similarly, the kNN classifier is based on the Euclidean distance to determine the class that best approximates the new instances. A small data variation in the feature under analysis will cause the voting function of this classifier to categorize the incoming instances correctly.

Although the SVM classifiers did not perform as well as the remaining MLCs, it still achieved the AUC score of 0.86 in the D2 data set, which is a reasonable result. This classifier uses the margin separation of the classes in the entire mapping of the data from a nonlinear space to a linearly separable one. According to the obtained results (worst on both data sets), this transformation makes this classifier a nonpractical model for feature spaces with high data variations (nonlinear class separation).

In order to compare the performance of the proposed descriptor against previously developed approaches available in the literature, we computed the ACC metric of the best scenario since most of the previous works use this parameter to measure the performance of their developed methods. In this sense, an ACC value of 95% was obtained by the FFBP ANN classifier in combination with the proposed descriptor output. This value overcomes the ACC results presented in similar works, such as 94% obtained by using a Hidden Markov model on a data set extracted from Llaima volcano, Chile [25], 94% obtained by using a combined model of RF and SVM classifiers on a data set of Ubinas volcano, Perú [37], and 90%, 94%, and 92% obtained by using deep learning models, such as recurrent neural network, long-short term memory, and gated recurrent unit, respectively, on a data set from Deception Island volcano, Antarctica [38]. These results indicate that the proposed descriptor is capable of providing competitive performance in the classification of volcanic seismic events compared with state-of-the-art methods.

IV. Conclusion and Future Work

In this article, we propose a new volcanic seismic signal descriptor to improve the AUC scores in the classification of LP and VT seismic events. The volcano seismic event signals are represented by the new descriptor from a different and novel point of view that involves image processing techniques instead of classic seismic signal processing strategies, such as frequency or scale analysis. The new representation transforms the segmented seismic event pattern in a gray-level spectrogram image into a new feature space involving 17 features computed from the intensity statistics, shape, and texture. The descriptor validation was based on two stages. First, the performance of the proposed descriptor for correctly determining the event pattern was evaluated using a seismic signal database with 637 instances, reaching an ACC value of 96%. Second, the descriptor output was validated using five different MLCs on two experimental data sets, containing feature vectors of signals without and with overlapping, having 598 and 637 instances in the D1 and D2 data sets, respectively. According to the AUC metric, all the MLCs obtained successful results. However, the best classification performance was acquired by the FFBP ANN classifier, reaching the higher AUC values of 0.96 and 0.95 for the D1 and D2 data sets, respectively. The poorest classification performance was that of the SVM classifier, reaching AUC values of 0.91 and 0.87 for the D1 and D2 data sets, respectively. This classifier was particularly sensitive to the overlapped seismic events in the D2 data set. These results indicate that the proposed descriptor correctly represents the seismic events in a new and different feature space, and its output provides competitive feature vectors to classify volcanic seismic events; it is also invariant across different MLCs.

As future work, we plan to implement two significant improvements to the proposed descriptor. First, we will modify the seismic event pattern determination step to increase the segmentation ACC on possible overlapped seismic events. This change could help to improve the classification performance on those MLCs sensitive to this effect (i.e., SVMs). Second, we will perform a correlation analysis based on the Pearson coefficient in the set of computed features to determine the optimal subset of features to be used in the classification of LP and VT seismic events. This analysis will allow us to reduce the dimension of the descriptor output and to improve the processing time. We also plan to increase the samples per class to compensate for the imbalance of instances between classes as well as include the processing of other seismic event types, such as tremors, very LP, explosions, hybrid, regional earthquakes, and teleseismic events.

Acknowledgment

The seismic data used in this article were provided by the Instituto Geofísico, EPN. P. Mothes helped to revise this text.

References

[1] U. S. Geological-Survey. *Volcano Hazards Program*. Accessed: May 18, 2019. [Online]. Available: https://volcanoes.usgs.gov/vhp/monitoring.html

[2] M. Malfante, M. Dalla Mura, J.-P. Metaxian, J. I. Mars, O. Macedo, and A. Inza, "Machine learning for volcano-seismic signals: Challenges and perspectives," *IEEE Signal Process. Mag.*, vol. 35, no. 2, pp. 20–30, Mar. 2018.

[3] R. Soto, F. Huenupan, P. Meza, M. Curilem, and L. Franco, "Spectro-temporal features applied to the automatic classification of volcanic seismic events," *J. Volcanol. Geotherm. Res.*, vol. 358, pp. 194–206, Jun. 2018. [Online]. Available: http://www.sciencedirect.com/science/article/pii/S0377027318300301

[4] M. Bicego, J. M. Londoño-Bonilla, and M. Orozco-Alzate, "Volcano-seismic events classification using document classification strategies," in *Image Analysis and Processing*, V. Murino and E. Puppo, Eds. Cham, Switzerland: Springer, 2015, pp. 119–129.

[5] Y. Rizk, H. Partamian, and M. Awad, "Toward real-time seismic feature analysis for bright spot detection: A distributed approach," *IEEE J. Sel. Topics Appl. Earth Observat., Remote Sens.*, vol. 11, no. 1, pp. 322–331, Jan. 2018.

[6] M. Curilem *et al.*, "Improving the classification of volcanic seismic events extracting new seismic and speech features," in *Progress in Pattern Recognition, Image Analysis, Computer Vision, and Applications*, M. Mendoza and S. Velastín, Eds. Cham, Switzerland: Springer, 2018, pp. 177–185.

[7] R. Lara-Cueva, D. S. Benitez, V. Paillacho, M. Villalva, and J. L. Rojo-Alvarez, "On the use of multi-class support vector machines for classification of seismic signals at cotopaxi volcano," in *Proc. IEEE Int. Autumn Meeting Power, Electron. Comput. (ROPEC)*, Nov. 2017, pp. 1–6.

[8] J. Demšar, "Statistical comparisons of classifiers over multiple data sets," *J. Machine Learn. Res.*, vol. 7, pp. 1–30, Jan. 2006.

[9] M. Hollander, D. A. Wolfe, and E. Chicken, *Nonparametric Statistical Methods*. Hoboken, NJ, USA: Wiley, 1999.

[10] A. V. Oppenheim, *Applications of Digital Signal Processing*. Englewood Cliffs, NJ, USA: Prentice-Hall, Inc., 1978, p. 510.

[11] E. C. Ifeachor and B. W. Jervis, *Digital Signal Processing: A Practical Approach*. London, U.K.: Pearson, 2002.

[12] J. F. Kaiser, "Nonrecursive digital filter design using the I_0-sinh window function," in *Proc. IEEE Int. Symp. Circuits Syst.*, San Francisco CA, USA, Apr. 1974, pp. 20–23.

[13] N. Otsu, "A threshold selection method from gray-level histograms," *IEEE Trans. Syst., Man, Cybern.*, vol. 9, no. 1, pp. 62–66, Jan. 1979.

[14] R. C. Gonzalez, R. E. Woods, and S. Eddins, *Digital Image Processing Using MATLAB*. Upper Saddle River, NJ, USA: Prentice-Hall, 2004.

[15] N. P. Pérez, M. A. G. López, A. Silva, and I. Ramos, "Improving the Mann–Whitney statistical test for feature selection: An approach in breast cancer diagnosis on mammography," *Artif. Intell. Med.*, vol. 63, no. 1, pp. 19–31, 2015. [Online]. Available: http://www.sciencedirect.com/science/article/pii/S0933365714001419

[16] A. K. Dhara, S. Mukhopadhyay, A. Dutta, M. Garg, and N. Khandelwal, "A combination of shape and texture features for classification of pulmonary nodules in lung CT images," *J. Digit. Imag.*, vol. 29, no. 4, pp. 466–475, Jan. 2016, doi: 10.1007/s10278-015-9857-6.

[17] Z. Zhang and E. Sejdić, "Radiological images and machine learning: Trends, perspectives, and prospects," *Comput. Biol. Med.*, vol. 108, pp. 354–370, May 2019. [Online]. Available: http://www.sciencedirect.com/science/article/pii/S0010482519300642

[18] R. M. Haralick, K. Shanmugam, and I. Dinstein, "Textural features for image classification," *IEEE Trans. Syst., Man, Cybern.*, vol. SMC-3, no. 6, pp. 610–621, Nov. 1973.

[19] R. A. Lara-Cueva, D. S. Benitez, E. V. Carrera, M. Ruiz, and J. L. Rojo-Alvarez, "Automatic recognition of long period events from volcano tectonic earthquakes at cotopaxi volcano," *IEEE Trans. Geosci. Remote Sens.*, vol. 54, no. 9, pp. 5247–5257, Sep. 2016.

[20] M. Curilem *et al.*, "Pattern recognition applied to seismic signals of the llaima volcano (Chile): An analysis of the events' features," *J. Volcanol. Geotherm. Res.*, vol. 282, pp. 134–147, Aug. 2014.

[21] R. Lara-Cueva, D. S. Benitez, V. Paillacho, M. Villalva, and J. L. Rojo-Alvarez, "On the use of multi-class support vector machines for classification of seismic signals at cotopaxi volcano," in *Proc. IEEE Int. Autumn Meeting Power, Electron. Comput. (ROPEC)*, Nov. 2017, pp. 1–6.

[22] B. Apolloni *et al.*, "Support vector machines and mlp for automatic classification of seismic signals at stromboli volcano," in *Proc. 19th Italian Workshop Neural Nets*, vol. 204. Amsterdam, The Netherlands: IOS Press, May 2009, p. 116.

[23] R. Lara-Cueva, E. V. Carrera, J. F. Morejon, and D. Benitez, "Comparative analysis of automated classifiers applied to volcano event identification," in *Proc. IEEE Colombian Conf. Commun. Comput. (COLCOM)*, Apr. 2016, pp. 1–6.
[24] R. A. Lara-Cueva, D. S. Benítez, E. V. Carrera, M. Ruiz, and J. L. Rojo-Álvarez, "Feature selection of seismic waveforms for long period event detection at cotopaxi volcano," *J. Volcanol. Geotherm. Res.*, vol. 316, pp. 34–49, Apr. 2016.
[25] S. M. Bhatti *et al.*, "Automatic detection of volcano-seismic events by modeling state and event duration in hidden Markov models," *J. Volcanol. Geotherm. Res.*, vol. 324, pp. 134–143, Sep. 2016. [Online]. Available: http://www.sciencedirect.com/science/article/pii/S0377027316301202
[26] J. Liu, H. A. Abbass, and K. C. Tan, "Evolutionary computation," in *Evolutionary Computation and Complex Networks*. Cham, Switzerland: Springer, 2019, pp. 3–22.
[27] K. M. Asim, A. Idris, T. Iqbal, and F. Martínez-Álvarez, "Seismic indicators based earthquake predictor system using genetic programming and AdaBoost classification," *Soil Dyn. Earthq. Eng.*, vol. 111, pp. 1–7, Aug. 2018. [Online]. Available: http://www.sciencedirect.com/science/article/pii/S0267726118301349
[28] P. Venegas, N. Perez, D. Benitez, R. Lara-Cueva, and M. Ruiz, "Combining filter-based feature selection methods and Gaussian mixture model for the classification of seismic events from cotopaxi volcano," *IEEE J. Sel. Topics Appl. Earth Observat., Remote Sens.*, vol. 12, no. 6, pp. 1991–2003, Jun. 2019.
[29] R. O. Duda *et al.*, *Pattern Classification and Scene Analysis*. New York, NY, USA: Wiley, 2000.
[30] A. Papadopoulos, D. I. Fotiadis, and A. Likas, "Characterization of clustered microcalcifications in digitized mammograms using neural networks and support vector machines," *Artif. Intell. Med.*, vol. 34, no. 2, pp. 141–150, Jun. 2005.
[31] S. Wang and R. M. Summers, "Machine learning and radiology," *Med. Image Anal.*, vol. 16, no. 5, pp. 933–951, Jul. 2012.
[32] Y. H. Hu and J.-N. Hwang, *Introduction to Neural Networks for Signal Processing*. Boca Raton, FL, USA: CRC Press, 2002, pp. 12–41.
[33] L. Breiman, "Random forests," *Machine Learn.*, vol. 45, no. 1, pp. 5–32, 2001.
[34] F. G. López, M. G. Torres, B. M. Batista, J. A. M. Pérez, and J. M. Moreno-Vega, "Solving feature subset selection problem by a parallel scatter search," *Eur. J. Oper. Res.*, vol. 169, no. 2, pp. 477–489, Mar. 2006.
[35] *version 9.6.0.1 (R2019a)*, The MathWorks, MATLAB, Natick, MA, USA, 2019.
[36] M. Hall, E. Frank, G. Holmes, B. Pfahringer, P. Reutemann, and I. H. Witten, "The WEKA data mining software: An update," *ACM SIGKDD Explorations Newslett.*, vol. 11, no. 1, pp. 10–18, 2009.
[37] M. Malfante, M. D. Mura, J. I. Mars, J.-P. Métaxian, O. Macedo, and A. Inza, "Automatic classification of volcano seismic signatures," *J. Geophys. Res., Solid Earth*, vol. 123, no. 12, pp. 10,645–10,658, Dec. 2018. [Online]. Available: https://agupubs.onlinelibrary.wiley.com/doi/abs/10.1029/2018JB015470
[38] M. Titos, A. Bueno, L. Garcia, M. C. Benitez, and J. Ibanez, "Detection and classification of continuous volcano-seismic signals with recurrent neural networks," *IEEE Trans. Geosci. Remote Sens.*, vol. 57, no. 4, pp. 1936–1948, Apr. 2019.

Noel Pérez (Member, IEEE) received the B.Eng. degree in computer science engineering, the M.Sc. degree in applied computer science, with a focus on digital image processing, pattern recognition, and machine learning, from the Universidad de Ciego de Avila, Ciego de Avila, Cuba, in 2005 and 2007, respectively, and the Ph.D. degree in data mining, pattern recognition, and machine learning from the University of Porto, Porto, Portugal, in 2015.

From 2008 to 2015, he was a Fellow Researcher with the Faculty of Engineering, Institute of Mechanical Engineering and Industrial Management (INEGI), University of Porto. From 2015 to 2017, he was with the Faculty of Sciences, Instituto de Telecomunicações, University of Porto, as a Post-Doctoral Fellow. Since 2017, he has been a full-time Professor with the Universidad San Francisco de Quito (USFQ), Quito, Ecuador. His research interests include digital image processing, data mining, pattern recognition, and machine learning.

Pablo Venegas received the B.Eng. degree in electronics engineering from the Universidad San Francisco de Quito (USFQ), Quito, Ecuador, in 2018.

His research interests include digital signal processing, real-time systems, and machine learning.

Diego Benítez (Senior Member, IEEE) received the B.Eng. degree in electrical engineering from the Escuela Politécnica Nacional, Quito, Ecuador, in 1994, and the M.Sc. and Ph.D. degrees in electrical engineering from the Institute of Science and Technology, University of Manchester, Manchester, U.K., in 1997 and 2001, respectively.

From 2005 to 2007, he was a Post-Doctoral Research Associate with Sensing, Imaging and Signal Processing Research Group, School of Electrical and Electronic Engineering, University of Manchester. From 2007 to 2012, he was a Senior Research Engineer with Bosch Research and Technology Center, Pittsburgh, PA, USA, where he was also an Academic Visitor with the Institute for Complex Engineered Systems and the Intelligent Infrastructure Research Laboratory (INFERLab), Carnegie Mellon University, Pittsburgh. From 2012 to 2014, he was a Visiting Research Scholar with the Universidad de las Fuerzas Armadas—ESPE, Sangolquí, Ecuador, through the Prometeo Program of SENESCYT, Quito, Ecuador. He is currently a full-time Faculty Member with the Universidad San Francisco de Quito (USFQ), Quito. His research interests include signal and image processing, and intelligent instrumentation and measurement systems for medical, energy management, security, and smart buildings applications.

Román Lara-Cueva (Senior Member, IEEE) received the B.Eng. degree in electronic and telecommunications engineering from the Escuela Politécnica Nacional, Quito, Ecuador, in 2001, the M.Sc. degree in wireless systems and related technologies from Politecnico di Torino, Turin, Italy, in 2005, and the M.Sc. and the Ph.D. degrees in telecommunication networks for developing countries from Rey Juan Carlos University, Fuenlabrada, Spain, in 2010 and 2015, respectively.

In 2002, he joined the Departamento de Eléctrica, Electrónica y Telecomunicaciones, Universidad de las Fuerzas Armadas—ESPE, Sangolquí, Ecuador, where he has been an Associate Professor since 2005, and he has been a Full Professor since 2016. He is the author or coauthor in 12 publicly funded research projects, and directed seven of them. He is currently the Head of the Ad Hoc Network Research Center (CIRAD) and the Smart Systems Research Group (WiCOM-Energy), Universidad de las Fuerzas Armadas—ESPE. His research interests include digital signal processing, smart cities, wireless systems, machine learning theory, and volcano seismology.

Mario Ruiz received the B.Eng. degree in geophysical engineering from the Escuela Politécnica Nacional, Quito, Ecuador, in 1992, the M.Sc. degree from the New Mexico Institute of Mining and Technology, Socorro, NM, USA, in 2004, and the Ph.D. degree in geological sciences from the University of North Carolina, Chapel Hill, NC, USA, in 2007.

He currently works as the Chair with the Instituto Geofísico, Politécnica Nacional, Quito. His research interest includes volcano seismology.